Journal of Power Sources 204 (2012) 220–229

Contents lists available at SciVerse ScienceDirect

Journal of Power Sources

journal homepage: www.elsevier.com/locate/jpowsour

Influence of nitric acid modification of ordered mesoporous carbon materials on their capacitive performances in different aqueous electrolytes

Jun-wei Lang[a], Xing-bin Yan[a,*], Wen-wen Liu[a,b], Ru-tao Wang[a,b], Qun-ji Xue[a]

[a] State Key Laboratory of Solid Lubrication, Lanzhou Institute of Chemical Physics, Chinese Academy of Sciences, Lanzhou 730000, PR China
[b] Gradute University of Chinese Academy of Sciences, Beijing 100080, China

ARTICLE INFO

Article history:
Received 14 September 2011
Received in revised form
17 December 2011
Accepted 20 December 2011
Available online 30 December 2011

Key words:
Ordered mesoporous carbon
Chemical modification
Capacitive performance
Supercapacitor

ABSTRACT

Two kinds of ordered mesoporous carbon (OMC), hexagonal mesoporous carbon CMK-3 and cubic mesoporous carbon CMK-8, are prepared by a hard template nanocasting method. Afterwards, nitric acid modification is conducted to explore the influence of surface functional groups on the supercapacitive characteristics of the OMC electrodes. The electrochemical performances of CMK-3, CMK-8, acid-modified CMK-3 (H-CMK-3) and acid-modified CMK-8 (H-CMK-8) electrodes are investigated in three-electrode cells using alkaline (2 M KOH), acidic (2 M H_2SO_4) and neutral (2 M Na_2SO_4) aqueous media. After nitric acid modification, the capacitive performances of two OMCs are improved in KOH, decreased in H_2SO_4, but showed no change in Na_2SO_4. The correlations among the change of surface functional groups after acid modification, electrolyte category and the capacitive performance of the OMCs are studied in detail. It can provide a guideline for proper usage of OMC-based materials for the next generation of supercapacitors.

1. Introduction

Because of the depletion of fossil fuels and increasing environmental concerns, one of the biggest challenges is to find and use an alternative energy conversion/storage system that can meet the present day power demands [1,2]. Supercapacitors, as a unique type of electrochemical energy storage devices, are not limited by the electrochemical charge transfer kinetics of batteries and thus can operate at very high charge and discharge rate [3–5]. Supercapacitors can be used either by themselves as the primary power source or in combination with fuel cells or batteries to deliver the high power needed during acceleration and to recover the energy during braking for automobiles [6,7].

At present, high-surface-area activated carbons (ACs) are still the predominant electrode materials for commercial supercapacitors [8–10]. However, the ultramicropores in ACs are inaccessible to the electrolyte ions, as well as the broad distribution of pore size, significantly decreasing the specific capacitance of ACs [11,12]. It is well known that the pore structures of carbon materials (micro-, meso- and macro-pore) critically affect their physicochemical properties, especially when the carbon materials serve as an electrode material involving the electrolyte accessibility, ion transportation, electron conductivity, etc. [13,14]. Thus, a combination of high surface area and optimal mesoporosity is highly desirable for carbon electrode materials to be used in high-performance supercapacitors. In this regard, ordered mesoporous carbons (OMCs) which possess well-ordered pore structures, narrow pore size distributions, high specific pore volumes and high specific surface areas, seem to be attractive candidates as electrode materials for supercapacitors [15,16].

Up to now, various methods such as soft template replicating, hard template nanocasting and self-assembly have been successfully employed to prepare OMCs with different porous structures [17]. Among them, a kind of ordered two-dimensional (2D) hexagonal mesoporous carbon, called CMK-3, has been widely investigated for electrical double-layer capacitors (EDLCs). CMK-3 is commonly prepared via a direct-templating nanocasting using a hexagonally ordered mesoporous silica SBA-15 as the hard template, and CMK-3 is the faithful replica of the mesoporous structure of SBA-15 [18,19]. Moreover, another kind of ordered 3D cubic mesoporous carbon, called CMK-8, can be prepared through the faithful inverse replica from another mesoporous silica KIT-6, which exhibits a typical 3D cubic structure (*Ia3d* symmetry) consisting of an interpenetrating bicontinuous network of channels [20,21]. Nevertheless, little attention has been paid to the supercapacitive properties of CMK-8 material.

As we know, besides the specific surface area and the pore characteristics, the energy performances of OMC-based supercapacitors are closely related to the surface functionalities as well as the selection of electrolytes. Generally, aqueous electrolytes such as KOH, H_2SO_4 and Na_2SO_4 solutions can provide high energy and power densities and be compatible with the

* Corresponding author. Tel.: +86 931 4968055; fax: +86 931 4968055.
E-mail address: xbyan@licp.cas.cn (X.-b. Yan).

0378-7753/$ – see front matter © 2011 Elsevier B.V. All rights reserved.
doi:10.1016/j.jpowsour.2011.12.044

supercapacitor industry [22,23]. In these aqueous electrolytes, the amount of stored energy can be significantly improved through pseudo-faradic reactions of active groups present on the carbon surfaces [24]. Recently, some works have showed that foreign atoms such as O, N, B and P can be introduced on the carbon surfaces by different oxidation procedures, and especially oxygen and nitrogen doping are favorable to enhance the capacitance [25–27]. The foreign atoms modify the electron donor/acceptor properties of the graphene layer, and are consequently expected to affect the charging of the electrical double layer and to give pseudo-capacitance faradaic reactions. Moreover, the heteroatoms in the carbon materials can also improve the wettability of the electrodes [26,28,29]. For example, Khomenko et al. [30] reported that higher capacitiance can be achieved for nanoporous carbon in both KOH and H_2SO_4 electrolytes by taking profit of different redox reactions. Ra et al. [22] reported that the N-containing groups of the polyacrylonitrile-based carbon nanofiber paper can noticeablely enhance its capacitance through a pseudo-faradaic contribution in KOH and H_2SO_4 electrolytes. Lota et al. [25] found that organic and neutral medium are not suitable for N-rich carbon electrodes.

Therefore, with a view to explore such new OMC-based supercapacitors, it is very necessary to study their electrochemical properties in different aqueous electrolytes, and to understand the electrochemical enhancement mechanism by acid-modification. However, to our knowledge, few studies have been reported on the influence of acid modification of OMC materials on their electrochemical behaviors in different aqueous electrolytes.

Herein, powdery CMK-3 and CMK-8 were prepared through the hard-template nanocasting approach using SBA-15 and KIT-6 silica as the mother templates, respectively. Afterwards, the surface of the samples was modified by nitric acid. The present work is focused on the supercapacitive properties of the unmodified and acid-modified CMK-3 and CMK-8 in KOH, H_2SO_4 and Na_2SO_4 electrolytes. In such a way, it will be possible to understand the redox reaction of active groups, which could affect the capacitance of one OMC electrode in an electrolyte solution. Finally, a detailed electrochemical study in a three-electrode cell showed that after nitric acid modification, the capacitance performances of the two OMCs were improved in KOH, decreased in H_2SO_4, but showed no change in Na_2SO_4. The correlations among the acid-modification, electrolyte category and the capacitance performance of OMC provide a guideline for proper usage of OMC-based materials for the next generation of supercapacitors.

2. Experimental

Triblock poly (ethylene oxide)-b-poly (propylene oxide)-b-poly (ethylene oxide) copolymer Pluronic P123 (M_w = 5800 $EO_{20}PO_{70}EO_{20}$) was purchased from Aldrich Chemical Inc. Nitric acid (CP), Potassium hydroxide (CP) and anhydrous ethanol (CP) were purchased from Tianjin Chemical Reagents Company. The other chemicals were purchased from Sinopharm Chemical Reagent Co. Ltd. All of the chemicals were used as received without any further purification. Deionized water was used in all experiments. Powdery activated carbon (AC, Kuraray, Japan, YP17, 1519 $m^2\ g^{-1}$) is commercial product and used as electrode material without further treatment.

2.1. Preparation of ordered mesoporous carbon CMK-3

Mesoporous silica SBA-15 was prepared by hydrothermal synthesis according to established procedures. Ordered mesoporous carbon CMK-3 was synthesized by the nanocasting method using sucrose as a precursor and mesoporous silica SBA-15 as a hard template according to the literature [31,32].

2.2. Preparation of ordered mesoporous carbon CMK-8

The KIT-6 parent material was prepared by hydrothermal synthesis according to the established procedures. Mesoporous carbon CMK-8 was synthesized by the nanocasting process using sucrose as a precursor and mesoporous silica KIT-6 as the hard template according to the literature [21].

2.3. Chemical modification of CMK-3 and CMK-8

The CMK-3 carbon was chemically modified using HNO_3 solution. Briefly, 0.3 g of CMK-3 was suspended in 30 ml of concentrated HNO_3 (68 wt.%) and then refluxed at 60 °C for 2 h. After the mixture was cooled down to room temperature, it was filtered and washed with deionized water until the pH value of the filtrate was around 7. Then the product was dried at 80 °C for 24 h in air. The nitric-acid-modified CMK-3 carbon was denoted as H-CMK-3. The same post-synthesis activation was carried out for CMK-8 and the nitric-acid-modified CMK-8 carbon was denoted as H-CMK-8.

2.4. Structural characterization

Transmission electron microscopy (TEM) measurements were conducted on a JEM-2010 microscope operated at 200 kV, to reveal the ordered structures of the CMK-3 and CMK-8 samples. Small-angle powder X-ray diffraction (SA-XRD) patterns were recorded by a Bruker D8 powder X-ray diffractometer using Cu Kα radiation. The chemical compositions of the samples were analyzed by Fourier transformation infrared spectroscopy (FTIR) using a Bruker IFS66V FTIR spectrometer. Nitrogen adsorption–desorption isotherm measurements were performed on a Micromeritics ASAP 2020 volumetric adsorption analyzer at 77 K. The Brunauer–Emmett–Teller (BET) method was utilized to calculate the specific surface area of each sample and the pore-size distribution was derived from the adsorption branch of the corresponding isotherm using the Barrett–Joyner–Halenda (BJH) method. The elemental analysis (C, H, O, N) for the OMCs was analyzed on varioELcube (Elementar Analysensysteme GmbH). The surface chemical compositions of the CMK-8 and H-CMK-8 were analyzed on a Perkin-Elmer PHI-5702 multifunctional X-ray photoelectron spectroscope (XPS, physical Electronics, USA) using Al Kα radiation of 1486.6 eV as the excitation source.

2.5. Electrode preparation and electrochemical measurements in three-electrode system

The working electrodes were prepared according to the method reported in the literature [33]. Typically, 80 wt.% of electroactive material was mixed with 7.5 wt.% of acetylene black (>99.9%) and 7.5 wt.% of conducting graphite in an agate mortar until a homogeneous black powder was obtained. To this mixture, 5 wt.% of poly(tetrafluoroethylene) was added with a few drops of ethanol. After briefly allowing the solvent to evaporate, the resulting paste was pressed at 10 MPa to nickel foam for the KOH and Na_2SO_4 media, and titanium foam for the H_2SO_4 media, respectively. The electrode assembly was dried for 16 h at 80 °C in air. Each carbon electrode contained about 8 mg of electroactive material for the KOH and Na_2SO_4 media, and 3 mg (because of the relatively low porosity and high rigidity for titanium foam, lower mass of the electroactive material is more easily to be pressed onto titanium foam) for the H_2SO_4 media, respectively. Each electrode had a geometric surface area of about 1 cm^2.

All the electrochemical measurements of each as-prepared electrode were carried out using an electrochemical working station (CHI660D, Shanghai, China) in a three-electrode system in 2 M KOH, 2 M H_2SO_4 and 2 M Na_2SO_4 electrolytes at room temperature. A

platinum gauze electrode (4 cm^2) and a saturated calomel electrode served as the counter electrode and the reference electrode, respectively. The cyclic voltammetry (CV) measurements were conducted at different scan rates ranging from 10 mV s^{-1} to 50 mV s^{-1}. Electrochemical impedance spectroscopy (EIS) measurements were recorded from 10 kHz to 100 mHz with an alternate current amplitude of 5 mV, the DC bias for the four OMC electrodes were −0.9 V, 0.1 V and −0.7 V in KOH, H_2SO_4 and Na_2SO_4 electrolyte, respectively. Galvanostatic charge/discharge measurements were run at different current densities ranging from 0.625 to 16.67 A g^{-1}. The corresponding specific capacitance was calculated from:

$$C \ \ (\mathrm{F\ g^{-1}}) = \frac{I}{(\mathrm{d}E/\mathrm{d}t) \times m} \approx \frac{I}{(\Delta E/\Delta t) \times m} \quad (1)$$

where C is the specific capacitance, I is the constant discharging current, dE/dt indicates the slope of the discharging curves, and m is the mass of the corresponding electrode material.

2.6. Electrochemical measurements in two-electrode system

Two symmetric capacitors (H-CMK-8/H-CMK-8 supercapacitor and commercial activated carbon (AC)/AC supercapacitor) were fabricated for comparison. The electrodes were prepared using nickel foam as the current collector; each electrode contained 4 mg of electrochemical active material and had a geometric surface area of about 1 cm^2. The cathode and anode electrode were pressed together and separated by a porous nonwoven cloth separator. The electrochemical measurements of the symmetric supercapacitors were carried out in 2 M KOH aqueous electrolyte and 1 M tetraethylammonium tetrafluoroborate/acetonitrile (Et_4NBF_4/AN) organic electrolytes using the electrochemical working station in a two-electrode cell at room temperature.

The specific capacitance of the supercapacitor cell can be evaluated from the charge/discharge test together with the following equation:

$$C_T \ \ (\mathrm{F\ g^{-1}}) = \frac{I\Delta t}{\Delta E \times m} \quad (2)$$

where I in A is the constant discharging current; Δt in s is the discharge time; ΔE in V is the potential window during the discharge process after IR drop; and m in g is the total mass of the two-electrode materials.

The specific capacitance of a single electrode in the supercapacitor cell can be calculated according to the following equation:

$$C_{sp} \ \ (\mathrm{F\ g^{-1}}) = 4 \times C_T \quad (3)$$

where C_T is the measured specific capacitance for the two-electrode cell.

The specific energy density and power density are defined as

$$E \ \ (\mathrm{Wh\ kg^{-1}}) = \frac{0.5 C_T V^2}{3.6} \quad (4)$$

$$P \ \ (\mathrm{kW\ kg^{-1}}) = \frac{E \times 3600}{t} \quad (5)$$

where V in V is the voltage change during the discharge process after IR drop, and t in s is the discharge time.

3. Results and discussion

3.1. Microstructural characterizations

The microstructures of the CMK-3 and CMK-8 carbon were examined by TEM. Fig. 1a shows a typical TEM image of CMK-3 carbon viewed along [1 0 0] direction. As the image shows, the ordered structure of CMK-3 is an exactly negative replica of SBA-15 with a hexagonal arrangement of cylindrical mesoporous tubes

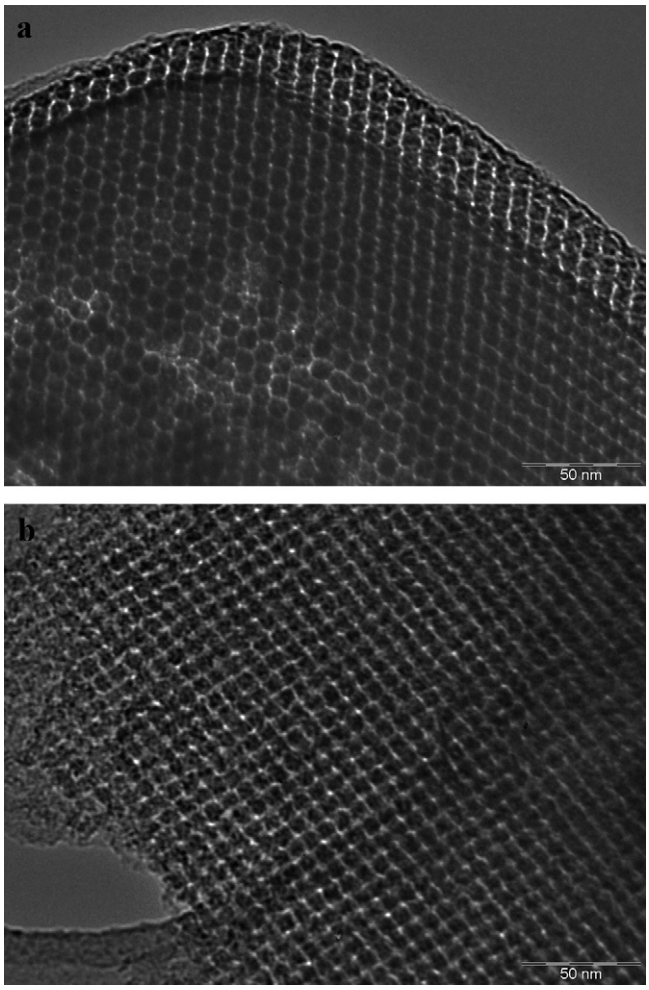

Fig. 1. TEM images of (a) the CMK-3 along [1 0 0] direction and (b) CMK-8 along [5 3 1] direction.

[34]. Fig. 1b shows a typical TEM image of the CMK-8 carbon viewed along [5 3 1] direction. As the image shows, the CMK-8 exhibits a long-range-ordered mesostructure in the whole domain, which indicates that the structure of the CMK-8 is exactly an inverse replica of KIT-6 which consists of 3D cubic (*Ia3d* symmetry) mesoporous tubes [35].

The carbon nanorods in the CMK-3 and CMK-8 are interconnected by spacers, which are constituted by the carbon that filled the channel-interconnecting micropores within the SBA-15 and KIT-6 walls. The ordered arrangement of the carbon nanorods in OMC materials gives rise to the well-resolved XRD peak. SA-XRD patterns of the CMK-3 and the CMK-8 are shown in Fig. 2. The clear (1 0 0) reflection of the CMK-3 reveals that the ordered two-dimensional hexagonal microstructure is well established. The XRD pattern of CMK-8 shows a strong diffraction peak at $2\theta = 1.04^\circ$, which is indexed as (2 1 1) diffraction of the 3D cubic *Ia3d* symmetry. Moreover, compared with the CMK-3 and CMK-8, there is no obvious change in intensity of the peaks for the H-CMK-3 and the H-CMK-8, respectively. It demonstrates that the ordered mesoporous structure can be well preserved after the acid modification.

The acid modification of the OMC materials can significantly affect the surface functionality. The FTIR measurements were employed to monitor chemical composition changes on the channel surface of the CMK-3 and CMK-8 before and after acid modification. Fig. 3 shows the FTIR spectra of CMK-3, H-CMK-3, CMK-8 and H-CMK-8. A broad band at around 3432 cm^{-1} is observed in all the four samples, which is mainly caused by the O—H

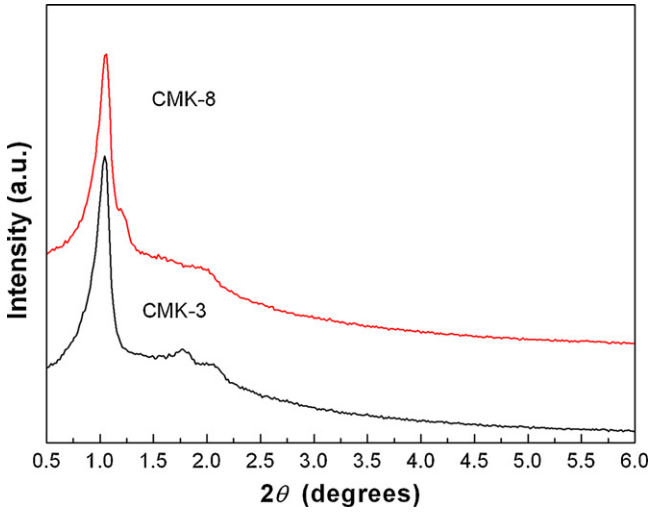

Fig. 2. The small-angle XRD patterns of the CMK-3 and the CMK-8.

stretching vibration of the adsorbed water molecules. The broad band at 1128 cm^{-1} is caused by the stretching vibration of the C—O bonds. In addition, the C=O stretching vibrations related to carbonyl and/or carboxyl groups can be found at around 1730 cm^{-1} [36]. The spectrum of the acid-modified OMC is similar to that of the unmodified OMC, except for stronger intensity of the peak at 1730 cm^{-1} for the acid-modified OMC, indicating more oxygen-containing functional groups existing on the channel surface of the H-CMK-3 and H-CMK-8 carbon.

Because the only difference between the CMK-3 and CMK-8 lies in their mesoporous structures, the change in the chemical compositions through the same acid modification should be identical. Thus, the chemical composition changes of C, H, O and N of CMK-8 and H-CMK-8 were monitored by elemental analysis, and XPS measurements were employed to monitor the changes of the surface functional groups of the CMK-8 through acid modification. Fig. 4 shows the well-fitted C_{1s} XPS spectrum of the CMK-8 and the H-CMK-8 and the corresponding analytic results are summarized in Table 1. As shown in Fig. 4a, the C_{1s} XPS spectrum of the CMK-8 can be divided into four different peaks, which corresponds to the signal of C=C bonds (284.4 eV), C—O bonds (286.3 eV), C=O bonds (287.5 eV), and O—C=O bonds (289.0 eV). Compared with the

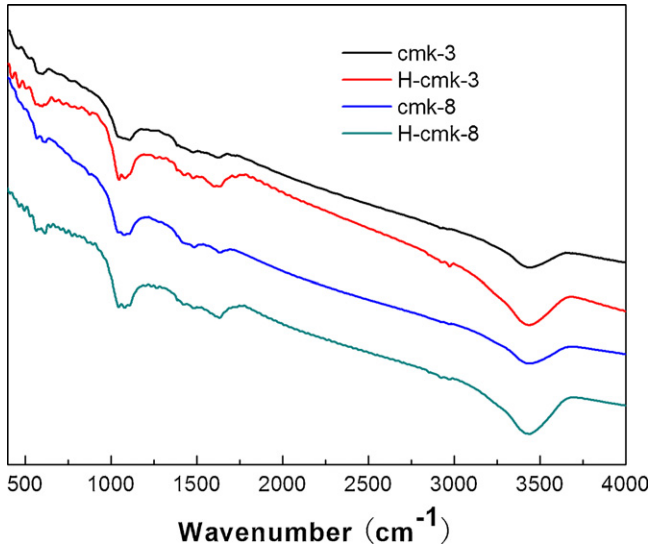

Fig. 3. The FTIR spectra of the CMK-3, H-CMK-3, CMK-8 and H-CMK-8.

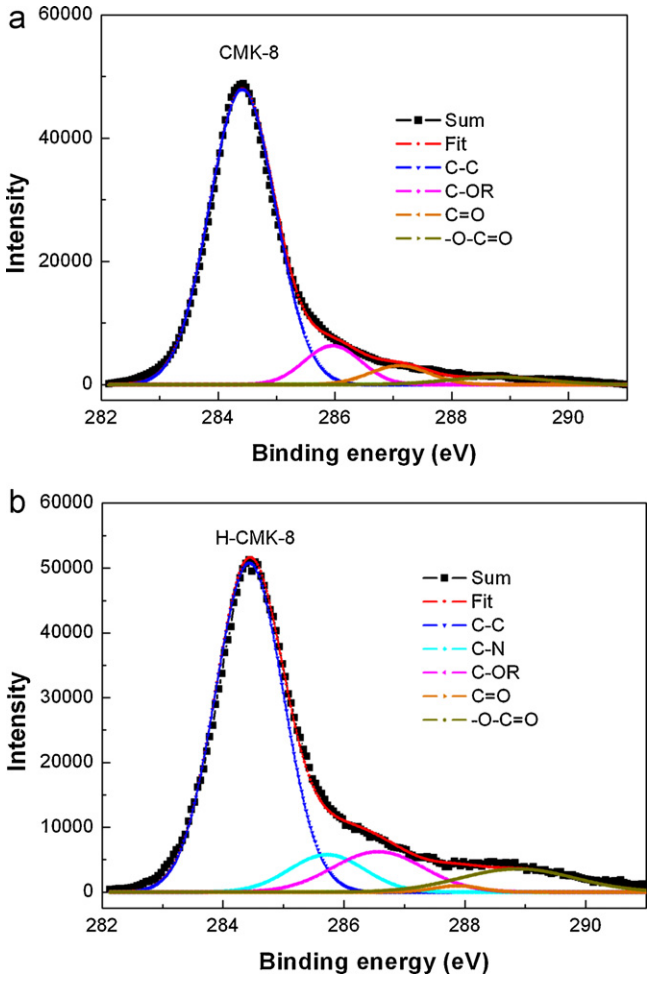

Fig. 4. C_{1s} XPS spectra of (a) the CMK-8 and (b) the H-CMK-8.

CMK-8, although the four components in the C_{1s} XPS spectrum of the H-CMK-8 are still present, their intensities undergo obvious changes. Concretely, the intensity of pyrone-like functionalities (C—O and O—C=O) is increased, but the intensity of quinine-like functionality (C=O) is decreased after modification [23,30]. Also, a new peak attributed to C—N bonds (285.6 eV) appears which indicates the incorporation of nitrogen via nitric acid treatment. Moreover, as shown in Table 1, both the oxygen and nitrogen contents are increased after acid modification. These results indicate that the acid modification can significantly affect the amount of surface functionalities on the OMC materials. In fact, these N- and O-containing functional groups could have certain effects on their electrochemical capacitive behaviors.

The specific surface area and pore-size distribution analyses of the four OMC materials were conducted using N_2 adsorption and desorption experiments. Table 2 summarizes the specific surface area of the samples. It is obvious that the acid treatment leads to the slight decrease in the specific surface area. Nevertheless, the influence of physical characteristics is considered to be minor in this work, since the changes in porosity and pore size distribution caused by the acid treatment are not obvious.

3.2. Electrochemical tests in three-electrode system

CV and chronopotentiometry measurements were employed to evaluate the electrochemical properties and to calculate the specific capacitances of as-prepared four OMC electrodes. EIS was employed to further analyze the relationship between the

Table 1
Elemental analysis and XPS surface characterization of the CMK-8 and the H-CMK-8.

Sample	C at.%	H at.%	O at.%	N at.%	C=C (C—C) at.% (284.4 eV)	C—N at.% (285.6 eV)	C—OR at.% (286.3 ± 0.2 eV)	C=O at.% (287.5 ± 0.2 eV)	—O—C=O at.% (289.0 ± 0.2 eV)
CMK-8	90.2	1.29	8.51	0	83.0	0	9.3	4.7	3.0
H-CMK-8	74.4	1.68	23.1	0.82	71.2	8.7	11.1	1.0	8.0

resistance and the capacitance. In our experiments, the four OMC electrodes tested in the same electrolyte are prepared under the same conditions, i.e., the same electrode surface, the same thickness, the same mass percentage of OMC, and the same contact condition with the current collector. Therefore, any different result of the electrochemical characterization will be derived from the difference in the electrolytes and microstructures of the OMC materials.

3.2.1. Characterization in 2 M KOH electrolyte

Fig. 5a shows the CV curves of the CMK-3, CMK-8, H-CMK-3, and H-CMK-8 electrodes between −1.0 and 0 V (vs. SCE) at the scan rate of 10 mV s^{-1} in 2 M KOH aqueous electrolyte. It can be seen that the CV curves of the CMK-3 and CMK-8 electrodes both exhibit a symmetric rectangular shape without obvious redox peaks, indicating typical double-layer capacitance behavior [37]. Nevertheless, the CV curves of the H-CMK-3 and H-CMK-8 electrodes deviate from idealized double-layer behavior with a pair of broad, superimposed and reversible faradaic surface redox reactions, behaving as pseudo-capacitance. Moreover, it is clear that the H-CMK-3 and H-CMK-8 electrodes exhibit larger CV areas than those of the CMK-3 and CMK-8 electrodes, suggesting higher specific capacitances compared with the untreated CMK-3 and CMK-8, respectively.

The galvanostatic charge/discharge is the most reliable method for estimating supercapacitor performance in real applications. Fig. 5b shows the charge/discharge curves of the four electrodes within a potential window of −1.0 to 0 V at at a current density of 0.625 A g^{-1}. It can be observed that all shapes of the charge–discharge curves for the OMC electrodes are closely linear and show a typical triangle symmetrical distribution, displaying a good capacitive property. After the acid modification, the specific capacitance increases from 165 F g^{-1} to 210 F g^{-1} for the CMK-3 carbon and from 175.7 F g^{-1} to 246.3 F g^{-1} for the CMK-8 carbon, respectively. It suggests that the nitric acid modification can remarkably increase the specific capacitance of the pristine OMC electrodes.

It is known that the pyrone-like (C—O and O—C=O) and N-containing functionalities are active in alkaline electrolyte [23,30]. As shown in Table 1, the amounts of the C—O, O—C=O and N-containing groups on the OMC are increased after acid modification. Therefore, in our system, the enhancement of the specific capacitance is attributed to the increase of these pyrone-like and N-containing funtional groups, which are able to provide some pseudo-faradaic contribution in KOH through redox reactions of these functionalities on the surfaces of the H-CMK-3 and H-CMK-8.

To further understand the high rate capability of the OMC electrodes, the charge/discharge measurements were recorded at different current densities. Fig. 5c reveals that the values of the specific capacitance for the OMC electrodes are strongly dependent on the current density. In detail, the specific capacitance slightly decreases with the increase of the current density. Up to a relatively large current density of 6.25 A g^{-1}, nearly 77.9%, 79.2%, 77% and 73.4% of the initial value remain for the four electrodes, respectively. This indicates that the high rate capability of the CMK-3 and CMK-8 in KOH electrolyte can be preserved after surface acid treatment. The result also comfirms that all the OMC electrodes allow rapid ion diffusion and exhibit good electrochemical utilization.

The complex plane plots of the AC impedance spectra in KOH electrolyte for the four electrodes are shown in Fig. 6. For each sample, there is a semi-circle intersecting the real axis in the high frequency range, and the plot transforms to a vertical line with decreasing frequency. From the point intersecting with the real axis in the range of high frequency, the internal resistance (which is equal to R_b) of the electrode material includes the total resistances of the ionic resistance of the electrolyte, the intrinsic resistance of active material, and the contact resistance at the active material/current collector interface. Since only the electrochemical process occurring on the exterior surface of electrodes can be sensed at high frequencies, the semicircle is suggested to represent the faradic charge transfer resistance (R_{ct}) at the interface between the current collector and the OMC as well as that within the OMC material. So, the semicircle may be due to both faradaic reaction as well as to powder-like structure of the electrode. At the lower frequencies, a straight sloping line represents the diffusive resistance (Warburg's impendence) of the electrolyte in electrode pores and the proton diffusion in host material [38,39].

As the plots show, the H-CMK-3 electrode has smaller R_b (0.79 Ω) than that of the CMK-3 electrode (0.87 Ω), while the CMK-8 and H-CMK-8 electrodes have similar small R_b (0.79 Ω). Moreover, it is obvious that the diameters of the semicircles for the pristine CMK-3 and CMK-8 are decreased after acid modification, indicating the lower impedance on the electrode/electrolyte interfaces for the H-CMK-3 and H-CMK-8. These observations are strongly correlated with the increase of the total capacitance. In addition, four plots all show a Warburg angle higher than 45°, indicating the suitability of the OMCs as the electrode materials for supercapacitors.

The cycle life of the OMC electrodes was monitored by chronopotentiometry measurements at 1.25 A g^{-1} in 2 M KOH electrolyte. As shown in Fig. 7, at the initial stage, the specific capacitances of the OMC electrodes all decrease gradually with the increase of the cycle number. After the initial 200 cycles, the values of the specific capacitances for the OMC electrodes show almost no decay up to 2000 cycles. We believe that, when the OMC materials were soaked with the electrolyte, some micropores would be blocked by the electrolyte due to the effect of capillarity during the initial cycles. These blocked micropores would affect ion transport throughout the pore channels and result in the decreased capacitance. When the block-effect became balanceable, the values of

Table 2
Specific surface areas and specific capacitances of the OMC carbons.

Sample	BET specific surface area (m^2 g^{-1})	Specific capacitance in KOH electrolyte (F g^{-1})	Specific capacitance in H_2SO_4 electrolyte (F g^{-1})	Specific capacitance in Na_2SO_4 electrolyte (F g^{-1})
CMK-3	1410	165	247.8	82.3
H-CMK-3	1351	210	208.3	85.8
CMK-8	1321	175.7	239.2	100.5
H-CMK-8	1217	246.3	216	109

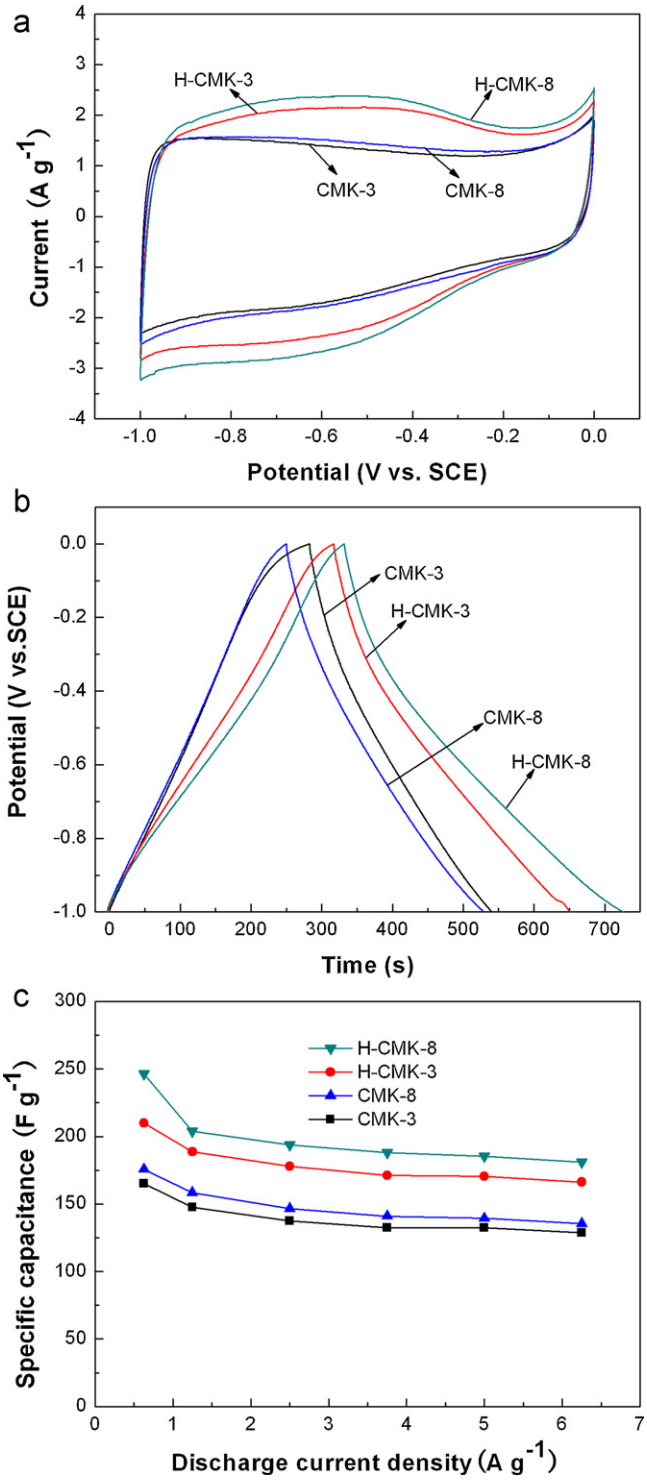

Fig. 5. (a) CV curves of the OMC electrodes at sweep rate of 10 mV s^{-1} in KOH electrolyte; (b) the charge–discharge curves of the OMC electrodes at a current density of 0.625 A g^{-1} in KOH electrolyte; (c) The specific capacitance of the OMC electrodes obtained in KOH electrolyte as a function of discharging current density.

the specific capacitances for the OMC electrodes showed almost no decay. It should be mentioned that, the real intrinsic mechanism is still not clear and further study needs to be carried out. For the CMK-3, CMK-8, H-CMK-3 and H-CMK-8 electrodes, the value of the final specific capacitance is 84.9%, 86%, 73.7%, and 75.3% of the initial value, respectively. This demonstrates that, within the voltage window of −1.0 to 0 V, the repeating charge–discharge behavior

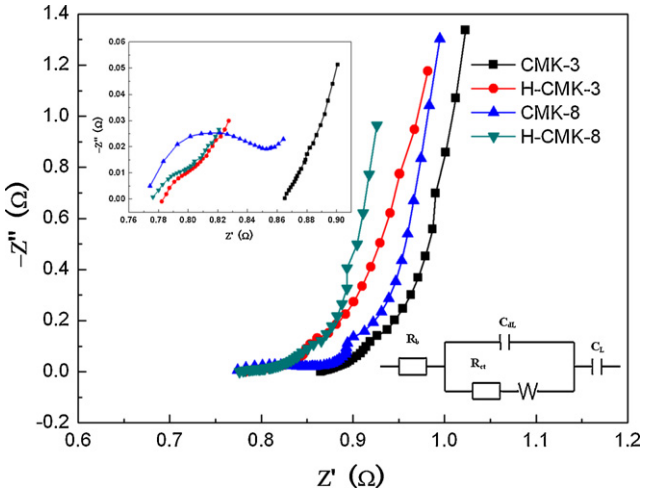

Fig. 6. Complex-plane impedance plots of the OMC electrodes in KOH electrolyte. The inset is the high frequency regions and the equivalent circuit.

does not seem to induce a significant structural change for the OMC electrodes. The long-term stability implies that four electrodes are good electrode materials for supercapacitors.

3.2.2. *Characterization in 2 M H_2SO_4 electrolyte*

Fig. 8a shows the CV curves of the CMK-3, CMK-8, H-CMK-3, and H-CMK-8 electrodes between −1.0 and 0 V (vs. SCE) at the scan rate of 10 mV s^{-1} in 2 M H_2SO_4 aqueous electrolyte. In addition to the current due to charging/discharging the electrical double-layer, cathodic and anodic humps are observed for the CMK-3 and CMK-8 electrodes. Generally, these peaks are attributed to the redox reactions of the O-containing (quinine-like) surface functionalities on the surface of the OMC materials. Moreover, these peaks are more pronounced for the H-CMK-3 and H-CMK-8 electrodes, which indicates a large faradaic contribution to the overall performance related to the O-containing (quinone-like) and N-containing surface functionalities as reported previously [26,28,40]. Fig. 8b shows the charge/discharge curves of the four electrodes within a potential window of −1.0 to 0 V at a current density of 1.67 A g^{-1} in 2 M H_2SO_4 electrolyte. After acid modification, the specific capacitance decreases from 247.8 F g^{-1} to 208.3 F g^{-1} for the CMK-3 carbon and from 239.2 F g^{-1} to 216 F g^{-1} for the CMK-8 carbon, respectively.

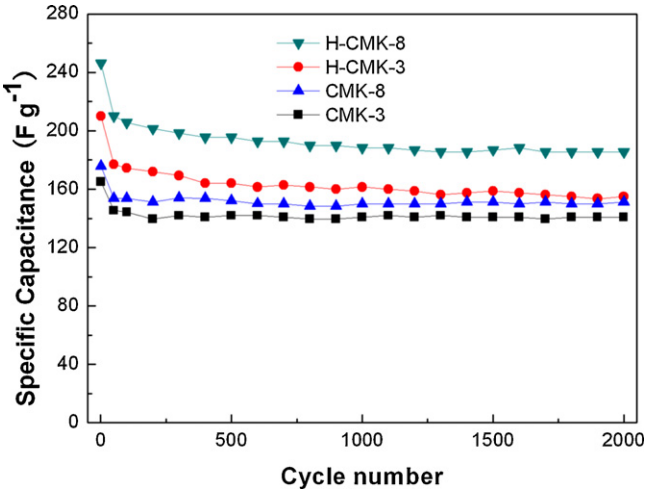

Fig. 7. Cycle life of the OMC electrodes at the current densities of 1.25 A g^{-1} in KOH electrolyte.

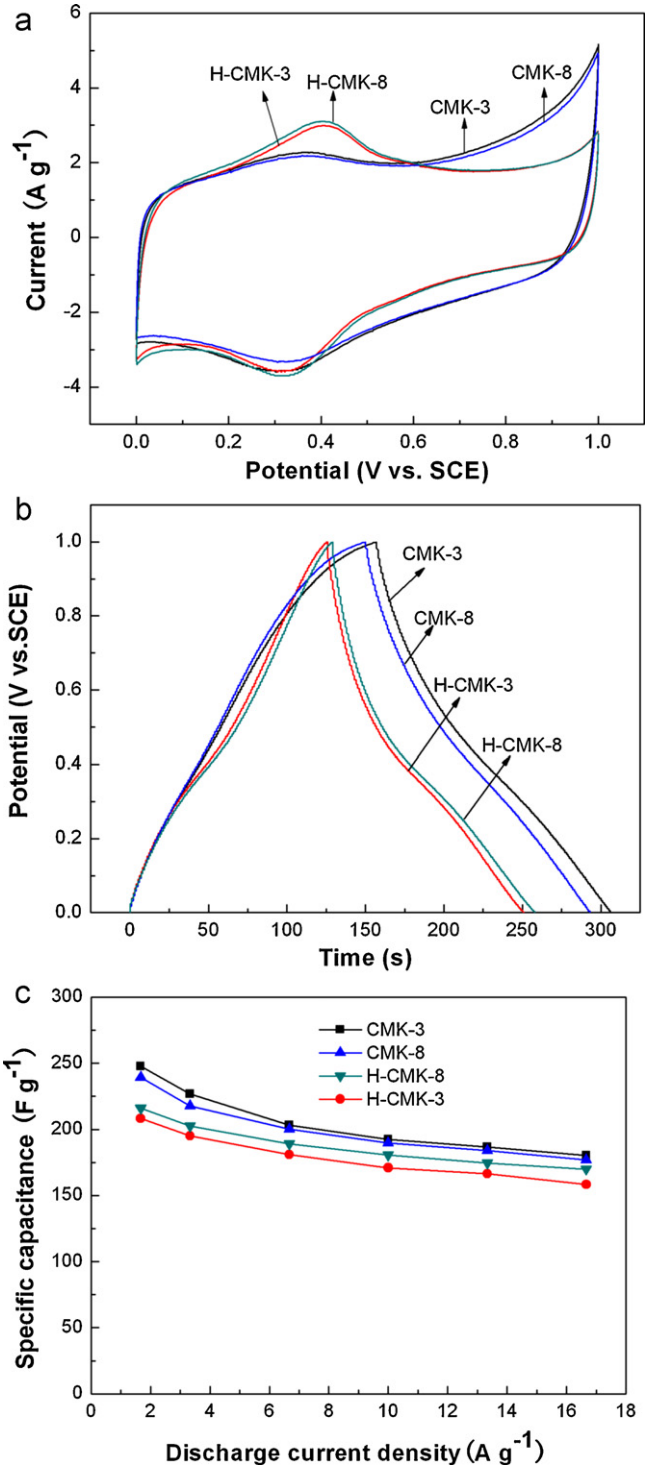

Fig. 8. (a) CV curves of the OMC electrodes at sweep rate of 10 mV s^{-1} in H_2SO_4 electrolyte; (b) the charge–discharge curves of the OMC electrodes at a current density of 1.67 A g^{-1} in H_2SO_4 electrolyte; (c) the specific capacitance of the OMC electrodes obtained in H_2SO_4 electrolyte as a function of discharging current density.

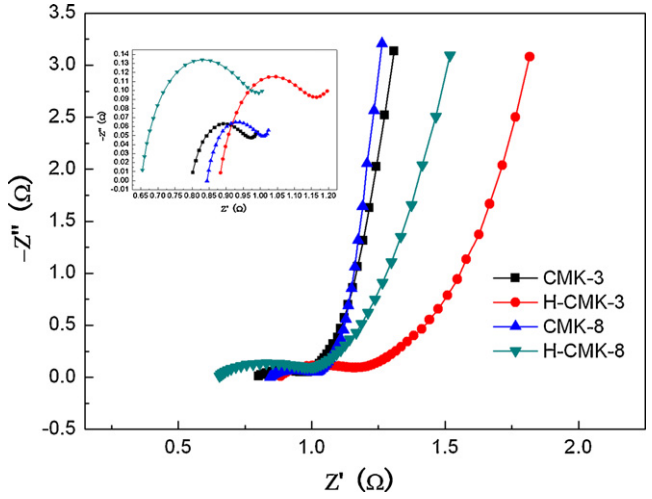

Fig. 9. Complex-plane impedance plots of the OMC electrodes in H_2SO_4 electrolyte. The inset is the high frequency regions.

It is well-known that the quinone-like (C=O) functionalities are electrochemically active in acid medium, the pyrone-like functionalities are electrochemically active in alkaline electrolyte, and the N-containing functionalities are electrochemically active in both acid and alkaline electrolyte. As shown in Fig. 4a, a small quantity of C=O groups are present at the surfaces of the OMC, even prior to HNO_3 activation. However, after acid modification, the amount of C=O groups is decreased. Also, a small quantity of C—N groups appear at the surface of H-CMK-3 and H-CMK-8. The decrease of the quinone-like (C=O) functionalities would provide negative pseudo-faradaic contributions, and the increase of the N-containing functionalities would provide positive pseudo-faradaic contributions. However, the capacitance increase resulting from the increase of N-containing groups cannot compensate for the loss of the capacitance due to the decreased quinone-like (C=O) functionalities. Thus, the capacitance values of the OMC were decreased in H_2SO_4 electrolyte.

Fig. 8c reveals that, up to a relatively large current density of 16.7 A g^{-1}, nearly 72.6%, 74%, 76% and 78.7% of the initial value remains for the four electrodes, respectively. This suggests that, although the supercapacitor performances of the OMC materials in 2 M H_2SO_4 solution cannot be improved by acid treatment, all the OMC materials are able to possess high rate capability in H_2SO_4 electrolytic medium, while keeping high values of specific capacitance.

The complex plane plots of the AC impedance spectra in H_2SO_4 electrolyte for the four electrodes are shown in Fig. 9. As the plots show, all the OMC electrodes have small R_b. Obviously, the diameters of the semicircles are expanded after acid modification, indicating lager impedance on the electrode/electrolyte interface. These observations are also strongly correlated with the decrease of the pseudo-capacitive contribution.

The cycle life of the OMC electrodes was monitored by the chronopotentiometry measurements at 3.33 A g^{-1} in 2 M H_2SO_4 electrolyte. As shown in Fig. 10, at the initial stage, the specific capacitances of the OMC electrodes all decrease gradually with the increase of the cycle number. After the initial 200 cycles, the specific capacitances for the OMCs have almost no decay up to 2000 cycles. For the CMK-3, CMK-8, H-CMK-3 and H-CMK-8 electrodes, the value of the final specific capacitance is 80.7%, 86.1%, 91.9% and 90.5% of the initial value, respectively. Also, the values of the specific capacitances for the four electrodes are almost the same as 200 F g^{-1} after 2000 cycles.

3.2.3. *Characterization in 2 M Na_2SO_4 electrolyte*

Fig. 11a shows the CV curves of the CMK-3, CMK-8, H-CMK-3, and H-CMK-8 electrodes between −0.9 and −0.3 V (vs. SCE) at the scan rate of 10 mV s^{-1} in 2 M Na_2SO_4 aqueous electrolyte. It can be seen that the CV curves of all the OMC electrodes show a typical rectangular shape, and no obvious faradaic current is observed in the voltammogram. Moreover, the CV area increases in the sequence of CMK-3 < H-CMK-3 < CMK-8 < H-CMK-8. However,

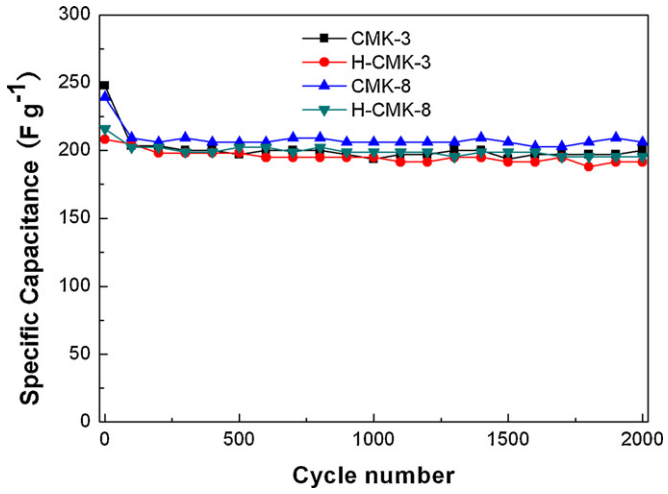

Fig. 10. Cycle life of the OMC electrodes at the current densities of 3.33 A g^{-1} in H_2SO_4 electrolyte.

the potential window of the OMC electrodes in Na_2SO_4 electrolyte is only 0.6 V, which is much lower than that in acidic and alkaline media. Fig. 11b shows the charge/discharge curves of the electrodes within a potential window of −0.8 to −0.3 V at the current density of 1.25 A g^{-1} in 2 M Na_2SO_4 aqueous electrolyte. The specific capacitance of the four electrodes is 82.3, 85.8, 100.5 and 109 F g^{-1}, respectively. The result indicates that the pseudocapacitive contribution of surface functional groups is negligible in neutral electrolyte. Fig. 11c reveals that, up to a relatively large current density of 6.25 A g^{-1}, 36.7, 24.2, 46.6 and 59.2% of the initial value remains for the four electrodes, respectively. The rate capability of the OMC in Na_2SO_4 electrolyte is very poor, indicating that Na_2SO_4 is not suitable for the OMC electrodes.

The complex plane plots of the AC impedance spectra in Na_2SO_4 electrolyte for the four electrodes are shown in Fig. 12. As the plots show, all the OMC electrodes have bigger R_b and R_{ct} than those in KOH and H_2SO_4 electrolytes, indicating the larger internal resistance and faradic charge transfer resistance.

The cycle life of the OMC electrodes was monitored at 1.25 A g^{-1} in 2 M Na_2SO_4 electrolyte. As shown in Fig. 13, for the four electrodes, the value of the specific capacitance is 70.9%, 60.7%, 70%, and 58.8% of the initial value, respectively. This demonstrates that the OMC electrodes have relatively poor long-term stability in Na_2SO_4 electrolyte.

From the above measurement results in the three electrolytes, it is pointed out that the OMC electrodes exhibit the highest capacitance values in H_2SO_4, lower capacitance values in KOH and the smallest capacitance values in Na_2SO_4. This result is in agreement with the literature data stating that the EDL capacitance values decreased in the sequence of H_2SO_4 > KOH > Na_2SO_4 because of the presence of protons or hydroxyl ions as mobile species with better ionic diffusion inside the pores than other ions. On the other hand, the conductivity of the Na_2SO_4 solution is approximately one order of magnitude less than that of H_2SO_4 solution or KOH solutions [23]. So the OMC electrodes have relatively low capacitance and poor long-term stability in Na_2SO_4 electrolyte.

3.3. Electrochemical tests in two-electrode system

We also investigated the electrochemical performance of the H-CMK-8 electrode in a two-electrode system (symmetric H-CMK-8/H-CMK-8 supercapacitor) and compared its supercapacitive performance (specific capacitance, energy density and power density) with commercial AC/AC supercapacitor. The

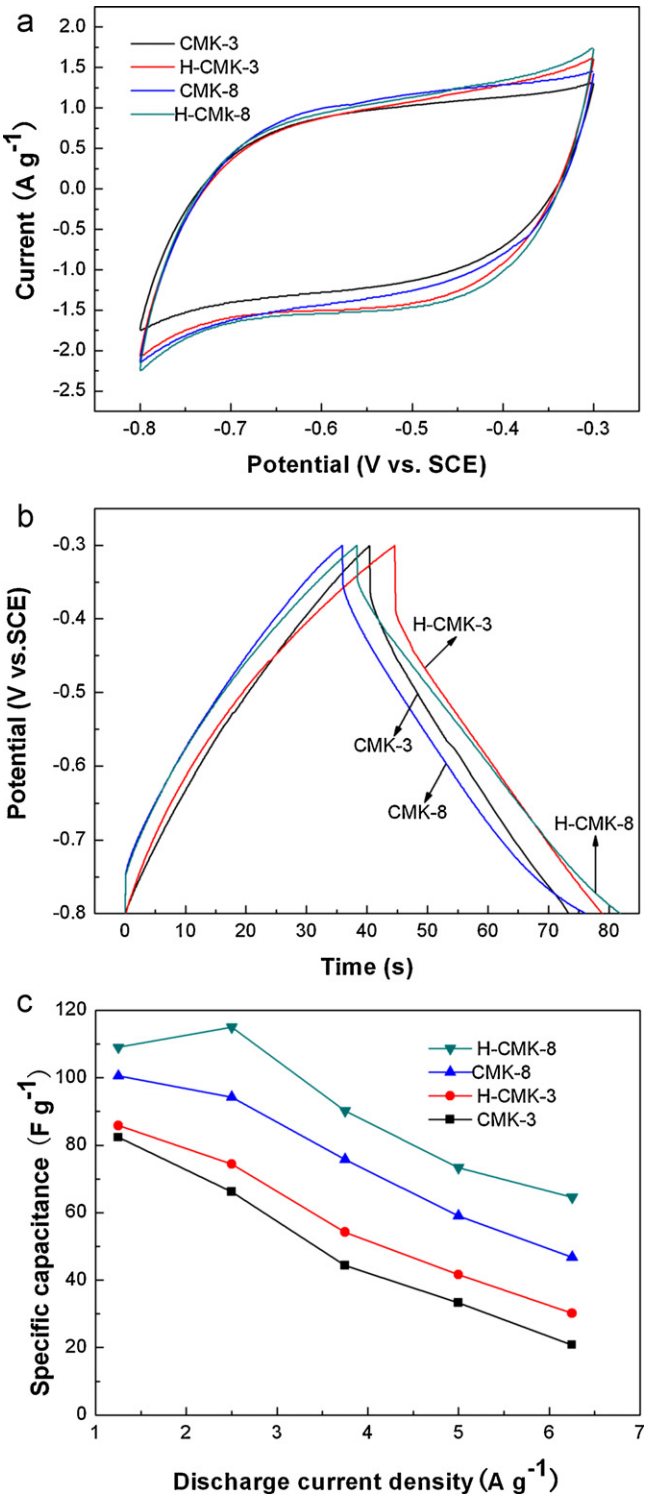

Fig. 11. (a) CV curves of the OMC electrodes at sweep rate of 10 mV s^{-1} in Na_2SO_4 electrolyte; (b) the charge–discharge curves of the OMC electrodes at a current density of 1.25 A g^{-1} in Na_2SO_4 electrolyte; (c) the specific capacitance of the OMC electrodes obtained in Na_2SO_4 electrolyte as a function of discharging current density.

electrochemical measurements were also carried out in 2 M KOH aqueous electrolyte and 1 M Et_4NBF_4/AN organic electrolyte at room temperature. Here, using the two-electrode symmetric system, the possible influence of area difference of the working and counter electrodes on the electrochemical properties would be excluded.

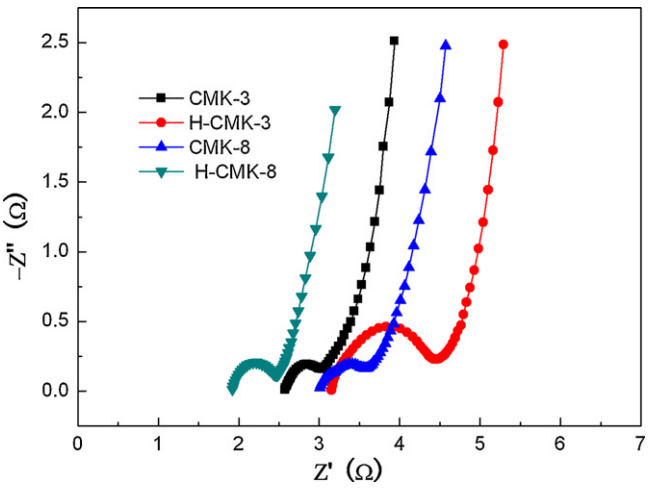

Fig. 12. Complex-plane impedance plots of the OMC electrodes in Na_2SO_4 electrolyte.

The values of specific capacitance of the cell and the single electrode in the cell, the energy density and power density depending on cell types and electrolytes are summarized in Table 3. The results show that the specific capacitance and energy density at the same power density of the H-CMK-8-based supercapacitor are much higher than those of the AC-based supercapacitor in KOH electrolyte. Therefore, the H-CMK-3 and H-CMK-8 materials could be used for the fabrication of carbon supercapacitors with KOH aqueous electrolyte. However, the specific capacitance of H-CMK-8 obtained from two-electrode system is lower than that obtained from three-electrode system. This phenomenon is very normal for electrode materials [41].

In Et_4NBF_4/AN electrolyte, the specific capacitance, energy density and power density of the two supercapacitors are almost the same. This is due to that the pseudo-capacitance of H-CMK-8 material is not reflected in the organic electrolyte. In other words, if using the organic electrolyte, the enhancement of acid-treatment in supercapacitive performance of CMK-8 cannot be realized. Since energy stored is related to the square of voltage, the energy density and power density of the supercapacitors in organic electrolyte are much higher than those in aqueous electrolyte. However, the specific capacitances of the H-CMK-8-based supercapacitor in KOH electrolyte are much higher than that in organic electrolyte. Thus,

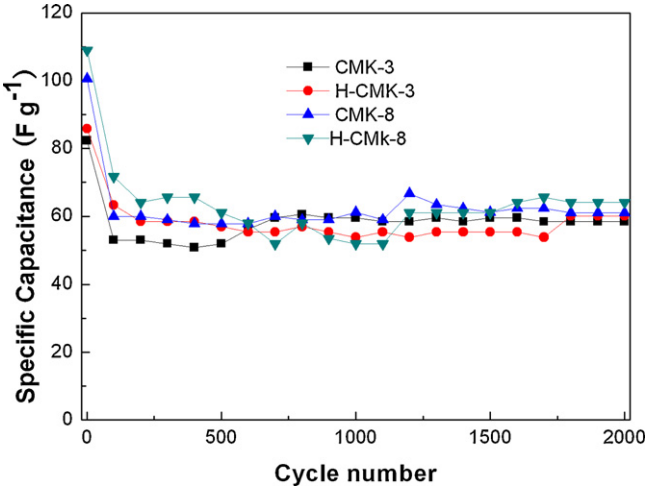

Fig. 13. Cycle life of the OMC electrodes at the current densities of 3.33 A g^{-1} in Na_2SO_4 electrolyte.

Table 3
Values of specific capacitance, energy density and power density depending on cell types and electrolytes.

Electrode material	KOH electrolyte				Et_4NBF_4/AN electrolyte			
	The specific capacitance of single electrode in three-electrode cell ($F g^{-1}$)	Two-electrode cell			Two-electrode cell			
		The specific capacitance of single electrode in two-electrode cell ($F g^{-1}$)	The specific capacitance of the cell ($F g^{-1}$)	Energy density ($Wh kg^{-1}$) and Power density ($W kg^{-1}$) at the current density of 0.5 A g^{-1}	The specific capacitance of single electrode in two-electrode cell ($F g^{-1}$)	The specific capacitance of the cell ($F g^{-1}$)	Energy density ($Wh kg^{-1}$) and Power density ($W kg^{-1}$) at the current density of 0.5 A g^{-1}	Energy density ($Wh kg^{-1}$) and Power density ($W kg^{-1}$) at the current density of 10 A g^{-1}
H-CMK-8	246	187	46.8	6.33/246.5	100	25	29.36/726.5	8.79/8795
AC	135	107	26.8	3.62/246.3	100.8	25.2	29.8/728.5	8.98/8829

such supercapacitors with aqueous electrolyte are suitable for some special use condition in which the capacitance demand is higher than energy density demand.

4. Conclusions

In summary, four OMCs, unmodified and nitric acid-modified CMK-3 and CMK-8 are prepared to study the influence of surface functional groups on the supercapacitive characteristics of the OMC electrodes in KOH, H_2SO_4 and Na_2SO_4 aqueous electrolytes. The results revealed that supercapacitive characteristics of the OMC electrodes are closely related to the kind and amount of the surface functional groups. In KOH electrolyte, the increased pyrone-like (C—O and O—C═O) and the N-containing functionalities are involved in redox reactions giving certain pseudo-faradaic contributions, which led to the result that the specific capacitances of the CMK-3 and CMK-8 are improved after nitric acid modification. However, in H_2SO_4 electrolyte, due to the decrease of the amount of quinone-like functionalities, the specific capacitances of the CMK-3 and CMK-8 are decreased after nitric acid modification. Furthermore, the influence of pseudo-faradic reactions is negligible in neutral electrolyte, even if the OMCs possess plentiful surface O- and N-containing functionalities. In addition, all the OMC materials are able to possess high rate capability both in KOH and H_2SO_4 electrolytic media, while keeping high values of specific capacitance. The worst capacitive performances are obtained in Na_2SO_4 electrolyte, suggesting that the neutral medium is not suitable for OMCs electrodes.

Acknowledgment

This work was supported by the Top Hundred Talents Program of Chinese Academy of Sciences and the Postdoctoral Science Foundation of China (20100480728).

References

[1] M. Winter, R.J. Brodd, Chem. Rev. 104 (2004) 4245–4269.
[2] P. Simon, Y. Gogotsi, Nat. Mater. 7 (2008) 845–854.
[3] S.H. Aboutalebi, A.T. Chidembo, M. Salari, K. Konstantinov, D. Wexler, Energy Environ. Sci. 4 (2011) 1855–1865.
[4] Z.S. Wu, D.W. Wang, W.C. Ren, J.P. Zhao, G.M. Zhou, F. Li, H.M. Cheng, Adv. Funct. Mater. 20 (2010) 3595–3602.
[5] J.W. Lang, L.B. Kong, W.J. Wu, Y.C. Luo, L. Kang, Chem. Commun. 35 (2008) 4213–4215.
[6] C.G. Liu, Z.N. Yu, D. Neff, A. Zhamu, B.Z. Jang, Nano Lett. 10 (2010) 4863–4868.
[7] H.L. Wang, H.S. Casalongue, Y.Y. Liang, H.J. Dai, J. Am. Chem. Soc. 21 (2010) 7472–7477.
[8] C.T. Hsieh, Y.T. Lin, Microporous Mesoporous Mater. 93 (2006) 232–239.
[9] W. Lu, L.T. Qu, K. Henry, L.M. Dai, J. Power Sources 189 (2009) 1270–1277.
[10] V.V. Panic, R.M. Stevanovic, V.M. Jovanovic, A.B. Dekanski, J. Power Sources 181 (2008) 186–192.
[11] L.X. Li, H.H. Song, X.H. Chen, Electrochim. Acta 51 (2006) 5715–5720.
[12] X.C. Zhao, A.Q. Wang, J.W. Yan, G.Q. Sun, L.X. Sun, T. Zhang, Chem. Mater. 22 (2010) 5463–5473.
[13] H.J. Liu, X.M. Wang, W.J. Cui, Y.Q. Dou, D.Y. Zhao, Y.Y. Xia, J. Mater. Chem. 20 (2010) 4223–4230.
[14] Q.H. Guo, X.P. Zhou, X.Y. Li, S.L. Chen, A. Seema, A. Greiner, J. Mater. Chem. 19 (2009) 2810–2816.
[15] H.F. Li, R.D. Wang, R. Cao, Microporous Mesoporous Mater. 111 (2008) 32–38.
[16] D.C. Wu, X. Chen, S.H. Lu, Y.R. Liang, F. Xu, R.W. Fu, Microporous Mesoporous Mater. 131 (2010) 261–264.
[17] H.F. Li, S.M. Zhu, H.A. Xi, R.D. Wang, Microporous Mesoporous Mater. 89 (2006) 196–203.
[18] J. Zhang, L.B. Kong, J.J. Cai, H. Li, Y.C. Luo, L. Kang, Microporous Mesoporous Mater. 132 (2010) 154–162.
[19] J.C. Wang, X.F. Yu, Y.X. Li, Q. Liu, J. Phys. Chem. C 111 (2007) 18073–18077.
[20] M. Lezanska, J. Wloch, G. Szymanski, I. Szpakowska, J. Kornatowski, Catal. Today 150 (2010) 77–83.
[21] K.P. Gierszal, M. Jaroniec, T.W. Kim, J. Kim, R. Ryoo, New J. Chem. 32 (2008) 981–993.
[22] E.J. Ra, E. Raymundo-Piñero, Y.H. Lee, F. Béguin, Carbon 47 (2009) 2984–2992.
[23] M.P. Bichat, E. Raymundo-Piñero, F. Béguin, Carbon 48 (2010) 4351–4361.
[24] H.L. Wang, Q.M. Gao, J. Hu, Microporous Mesoporous Mater. 131 (2010) 89–96.
[25] G. Lota, E. Frackowiak, Fuel Cells 10 (2010) 848–855.
[26] D. Hulicova-Jurcakova, M. Seredych, G.Q. Lu, T.J. Bandosa, Adv. Funct. Mater. 19 (2009) 438–447.
[27] Y.R. Nian, H. Teng, J. Electroanal. Chem. 540 (2003) 119–127.
[28] F.B. Su, C.K. Poh, J.S. Chen, G.W. Xu, D. Wang, Q. Li, J.Y. Lin, X.W. Lou, Energy Environ. Sci. 4 (2011) 717–724.
[29] E. Frackowiak, Phys. Chem. Chem. Phys. 9 (2007) 1774–1785.
[30] V. Khomenko, E. Raymundo-Piñero, F. Béguin, J. Power Sources 195 (2010) 4234–4241.
[31] X.Y. Yuan, J.W. Lü, X.B. Yan, L.T. Hu, Q.J. Xue, Microporous Mesoporous Mater. 142 (2011) 754–758.
[32] X.B. Yan, L. Gottardo, S. Bernard, P. Dibandjo, A. Brioude, H. Moutaabbid, P. Miele, Chem. Mater. 20 (2008) 6325–6334.
[33] J.W. Lang, L.B. Kong, M. Liu, Y.C. Luo, L. Kang, J. Electrochem. Soc. 157 (2010) A1341–A1346.
[34] Y.G. Wang, L. Cheng, F. Li, H.M. Xiong, Y.Y. Xia, Chem. Mater. 19 (2007) 2095–2101.
[35] Y.F. Shi, Y. Meng, D.H. Chen, S.J. Cheng, P. Chen, H.F. Yang, Y. Wan, D.Y. Zhao, Adv. Funct. Mater. 16 (2006) 561–567.
[36] J. Zhang, L.B. Kong, J.J. Cai, Y.C. Luo, L. Kang, Electrochim. Acta 55 (2010) 8067–8073.
[37] Q.L. Du, M.B. Zheng, L.F. Zhang, Y.W. Wang, J.H. Chen, L.P. Xue, W.J. Dai, G.B. Ji, J.M. Cao, Electrochim. Acta 55 (2010) 3897–3903.
[38] M.W. Xu, D.D. Zhao, S.J. Bao, H.L. Li, J. Solid State Electrochem. 11 (2007) 1101–1107.
[39] S.S. Zhang, K. Xu, T.R. Jow, Electrochim. Acta 49 (2004) 1057–1061.
[40] H.A. Andreas, B.E. Conway, Electrochim. Acta 51 (2006) 6510–6520.
[41] M.D. Stoller, R.S. Ruoff, Energy Environ. Sci. 3 (2010) 1294–1301.